J Mater Sci: Mater Electron (2017) 28:15907–15914
DOI 10.1007/s10854-017-7486-1

A correlative study on strain and variation of coercive field in lead-free $(Na_{0.5}Bi_{0.5})TiO_3$–$Bi(Mg_{0.5}Zr_{0.5})O_3$–$Bi(Mg_{0.5}Ti_{0.5})O_3$ ternary system

D. E. Jain Ruth[1] · B. Sundarakannan[2]

Received: 4 April 2017 / Accepted: 5 July 2017 / Published online: 11 July 2017

Abstract Sodium bismuth titanate–bismuth magnesium zirconate–bismuth magnesium titanate (NBT–BMZ–BMT) lead-free ternary ceramics are prepared by solid-state reaction method. Consequence on structural, dielectric, ferroelectric properties and piezoelectric coefficient is investigated. Single phase rhombohedral R3c phase is retained in all poled samples. Coercive field decreases due to minimum homogeneous strain (δ) which facilitates domain reorientation and domain switching. Reduced homogeneous strain is the key factor which lowers the coercive field and enhances the dielectric constant. NBT–BMZ–BMT ternary ceramics reduces the coercive field and possesses high remnant polarization, dielectric constant and piezoelectric coefficient—the important requirement in functional devices.

1 Introduction

Piezoelectric ceramics are considered as functional materials, due to the unique coupling of electrical and mechanical stimulants and its tremendous applications in commercial and technological equipments such as piezoelectric motors, printing machines, thread guides, frequency filters, ultrasound imaging, high-power ultrasonic transducers, motors, transformers and positioning systems [1, 2]. Majority of the devices employ the well-known piezoelectric PZT based compositions with fine tuned properties using selective dopants, which contains 60 wt% of lead. But, the toxicity of lead leads to health hazards and environmental pollution [3–5]. Hence, a lot of research activities have been reported on lead-free piezoelectric ceramics with an objective to find an alternate material to PZT with comparable properties [2].

Researchers predict that sodium bismuth titanate (NBT) may become a possible substitute to PZT in deed of its high ferroelectric nature ($P_r = 38\ \mu C/cm^2$), Curie temperature ($T_c = 320\ °C$), medium piezoelectric coefficient ($d_{33} = 73 pC/N$) and reasonable depolarization temperature ($T_d = 120\ °C$) [2–8]. But its high coercive field ($E_c = 73$ kV/cm) is still a major drawback for application in functional devices.

Randall et al. [9], Shabbir et al. [10] and Suchomel et al. [11] have explored $(1-x)Bi(Mg_{1/2}Ti_{1/2})O_3$–$xPbTiO_3$ (BMT–PT) and $(1-x)Bi(Mg_{1/2}Zr_{1/2})O_3$–$xPbTiO_3$(BMZ–PT) as high temperature piezoelectric solid solutions and showed that these systems have significantly higher Curie temperature (T_C) than PZT making them superior for high temperature piezoelectric applications. But these systems contain $PbTiO_3$ (PT). Wang et al. [12], Ullah et al. [13] and Ruth et al. [14] have reported that $(Na_{0.5}Bi_{0.5})TiO_3$–$Bi(Mg_{0.5}Ti_{0.5})O_3$ [$(1-x)$NBT–xBMT] lead-free piezoelectric ceramics possess enhanced piezoelectric coefficient (d_{33}) and high Curie temperature. In $(1-x)(Na_{0.5}Bi_{0.5})TiO_3$–$Bi(Mg_{0.5}Ti_{0.5})O_3$ highest piezoelectric coefficient (d_{33}) is obtained for $x = 0.04$ mole fraction of BMT substitution in NBT [12–14]. Also, Ruth et al. [15] proposed that $(1-x)(Na_{0.5}Bi_{0.5})TiO_3$–$xBi(Mg_{0.5}Zr_{0.5})O_3$ [$(1-x)$NBT–xBMZ] solid solution exhibits enhanced piezoelectric coefficient, better ferroelectric properties and high transition temperature. In $(1-x)(Na_{0.5}Bi_{0.5})TiO_3$–$xBi(Mg_{0.5}Zr_{0.5})O_3$ [$(1-x)$NBT–xBMZ] solid

✉ D. E. Jain Ruth
hccjradp@gmail.com

[1] Department of Physics, School of Physical, Chemical & Applied Sciences, Pondicherry University, Puducherry 605014, India

[2] Department of Physics, Manonmaniam Sundaranar University, Tirunelveli, Tamil Nadu 627012, India

solution, highest piezoelectric coefficient and ferroelectric properties are obtained for $x=0.01$ mole fraction of BMZ substitution.

Several reports reveal that preferred piezoelectric, electromechanical, dielectric and ferroelectric properties can be achieved in ternary systems such as BNT–BKT–BT [16, 17], BNT–BKT–KNN [18, 19], BNT–BKT–NN [20, 21], BNT–BKT–BM [22]. Therefore, in the present work our objective is to know the changes in ferroelectric, dielectric properties namely remnant polarization (P_r), coercive field (E_c) dielectric constant (ε_r) and piezoelectric coefficient (d_{33}) in NBT–BMZ–BMT ternary system.

In the present work, $(1-x-y)(Na_{0.5}Bi_{0.5})TiO_3$–$xBi(Mg_{0.5}Ti_{0.5})O_3$–$yBi(Mg_{0.5}Zr_{0.5})O_3$ ternary ceramics is synthesized by solid state reaction method. Mole fraction of BMZ is kept constant as $y=0.005$ mole fraction and the mole fraction of BMT is varied (i.e. x) up to $x=0.025$. Effect of substitution on electrical properties is studied in relation with structural parameters. Also, a comparative study is carried out to study the major structural factor which influences the electrical properties in NBT–BMT, NBT–BMZ and NBT–BMT–BMZ systems. The indispensable factor for softening coercive field is analyzed in relation to intrinsic parameter homogeneous strain and rhombohedral lattice distortion. Moreover, NBT–BMZ–BMT ternary system was not reported to the best of author's knowledge.

2 Experimental

Conventional solid-state reaction method was used to synthesize NBT–BMZ–BMT ternary system. Flow chart (Fig. 1) shows the various steps followed for the preparation of ceramics. Using Archimedes principle densities of the pellets were found and the relative density of the pellets is above 96% of the theoretical density.

Powder X-ray diffraction, Raman spectra, frequency dependent dielectric, ferroelectric properties and piezoelectric constant (d_{33}) were measured for NBT–BMZ–BMT ternary system using the same condition and instruments which was reported in NBT–BMT and NBT–BMZ solid solutions [14, 15].

3 Results and discussion

X-ray diffraction patterns of $(1-x-y)$NBT–xBMT–yBMZ ternary poled ceramics with different mole fractions of BMT such as $x=0$, 0.005, 0.015 and 0.025 respectively are shown in Fig. 2. All the peaks are indexed to pseudocubic phase. No unindexed peaks are noticed and hence the synthesized ceramics are phase pure. Absence of impurity peaks reveals that the samples are in single phase. Remarkable features of rhombohedral structure is doublet nature of $\{110\}_{pc}$ peak and well-defined splitting of $\{111\}_{pc}$ and $\{211\}_{pc}$ peaks. Clear separation of $\{111\}_{pc}$ and $\{211\}_{pc}$ peaks (shown as encircled in Fig. 2) and bifurcation of $\{110\}_{pc}$ peak indicates that the poled ceramics are in rhombohedral phase as reported by Rao and Ranjan [23]. Presence of a weak peak referred to be superstructure reflection at a diffraction angle of around $2\theta=38.28°$ is a unique feature of R3c space group similar to Aksel et al. [24] and Jones et al. [25] investigations. Couplet nature of $\{110\}_{pc}$ peak, distinct cleavage of $\{111\}_{pc}$ and $\{211\}_{pc}$ peaks and superstructure reflection are ascertained in poled samples up to $x=0.025$ mole fraction. Hence the poled ceramics retains rhombohedral R3c structural symmetry up to $x=0.025$ mole fraction.

Change in peak intensity and d-spacing between $\{111\}$ and $\{11-1\}$ planes prompts rhombohedral lattice distortion and homogeneous strain of the lattice. Rhombohedral lattice distortion is calculated using the formula $\delta_r=(9/8)(d_{111}/d_{-111}-1)$. Homogeneous strain is deviation of the angle α from 90° and is found as $\delta=\pi/2-\alpha$ [26]. Figure 3 shows the rhombohedral lattice distortion and homogeneous strain of NBT–BMT–BMZ ternary poled ceramics. It is found that both parameters decrease gradually on substitution of BMT in NBT–BMZ ceramics.

Room temperature Raman spectra of $(1-x-y)$ NBT–xBMT–yBMZ ternary poled ceramics is shown in Fig. 4. Raman spectrum is deconvoluted using Lorenztian function equation $I = y_0 + \sum_{1=0}^{10} \frac{2A_i}{\pi} \frac{\Gamma_i}{4(\omega-\omega_{ci})2+\Gamma_i^2}$, A_i is area of the peak, ω_{ci} is peak center, Γ_i full-width at half-maximum of ith mode, y_0 is constant background. Raman spectrum is deconvoluted into sum of nine Lorenztians, one Lorenztian with center at 0 cm^{-1} for laser line to the raising background below 90 cm^{-1} and constant background.

The irreducible representation for rhombohedral (R3c) phase of NBT is $\Gamma_{30}=5A_1+5B_1+10E$. $4A_1+9E$ modes are both Raman and IR active and $5B_1$ modes are silent. One A_1+E modes are acoustic modes. Because of the long range Columbic force, all the optical modes split into longitudinal optical (LO) and transverse optical (TO) modes polarizations [27].

Kriesel and Bouvier [28] have reported that modes at the low wave number region below 150 cm^{-1}, are referred to be dominated by vibrations involving A-site cations (Na/Bi), mid wave number region (250–350 cm^{-1}) is attributed to vibrations associated with the BO_6 (TiO_6) octahedral and the high-wave number modes are dominated by vibrations of O^{2-} anions involving the most rigid cation–oxygen bonds inside the BO_6 octahedra of the perovskite. Similar broad peaks are obtained in BMT substituted NBT–BMZ system as previously reported systems which are the characteristic

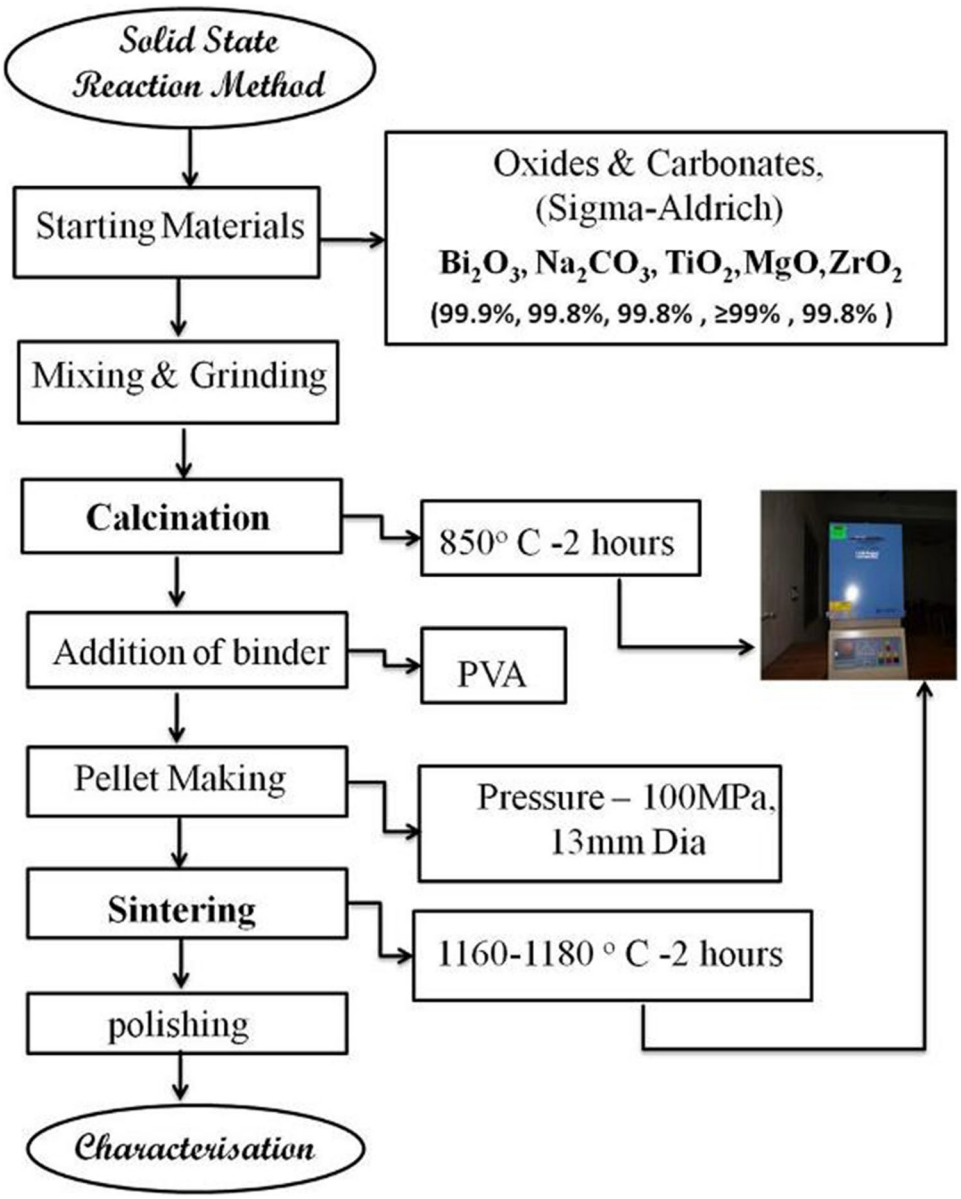

Fig. 1 Steps involved in solid state reaction method

nature of relaxor ferroelectrics [27–30]. Vibrational modes in the frequency range 109–134 cm^{-1} are dominated by Bi–O vibrations while the modes in 155–187 cm^{-1} are dominated by Na–O vibrations. TiO_6 vibrations are dominated in the frequency range 246–401 cm^{-1}. Oxygen atom vibrations are predominantly contributed to phonon frequencies in the range of 413–826 cm^{-1} [28–30]. No significant change in frequency modes and intensity is noticed in BMT substituted NBT–BMZ ceramics. Presence of all these vibrational modes is a signature to rhombohedral structural symmetry and confirms the structure observed from XRD of NBT–BMZ–BMT poled ceramics.

Frequency dependent dielectric constant (ε_r) and dielectric loss of $(1-x-y)$NBT–xBMT–yBMZ poled ceramics are shown in Figs. 5 and 6. Figure depicts that the dielectric constant and loss decreases as the frequency increases (Figs. 5, 6). Decrease in dielectric constant is a known fact that polarization does not occur simultaneously under the application of electric field. However, it is due to the inertia of dipoles and the delay in response towards the impressed alternating electric field which leads to decrease in ε_r and tan δ. At low frequencies, contribution from space charge polarization is dominant and hence dielectric constant is maximum. But as frequency increases, polarizations with large relaxation time cease to respond to the applied electric field and hence dielectric constant decreases. Presence of sharp lower kink in the dielectric constant and upper kink in the tan δ curve (shown as encircled in Figs. 5, 6) suggests the resonance peak at these frequencies [31]. Decrease of tan δ with the increase in frequency after

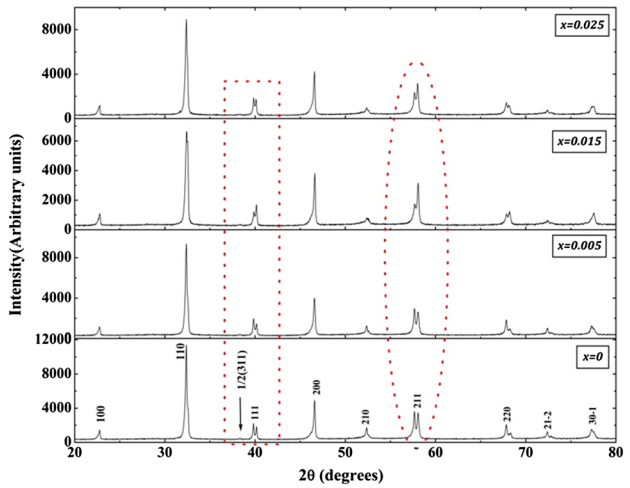

Fig. 2 X-ray diffraction patterns of $(1-x-y)$NBT–xBMT–yBMZ ternary poled ceramics with $x=0$, 0.005, 0.015 and 0.025

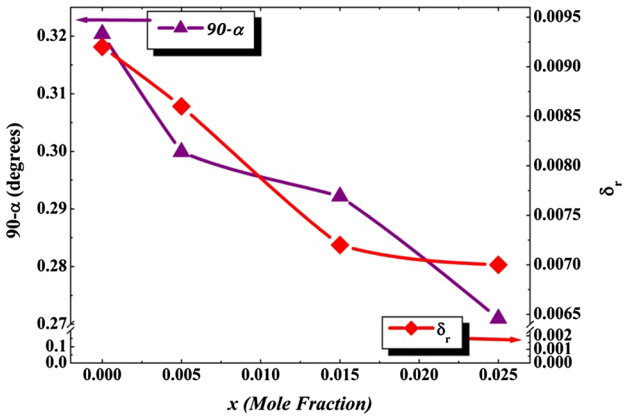

Fig. 3 Homogeneous strain (δ) and lattice distortion (δ_r) of $(1-x-y)$NBT–xBMT–yBMZ poled ceramics with various x

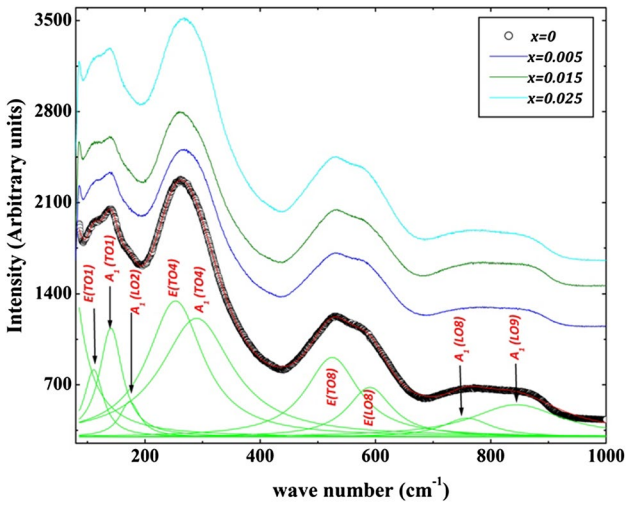

Fig. 4 Raman spectra of $(1-x-y)$NBT–xBMT–yBMZ poled ceramics with various x

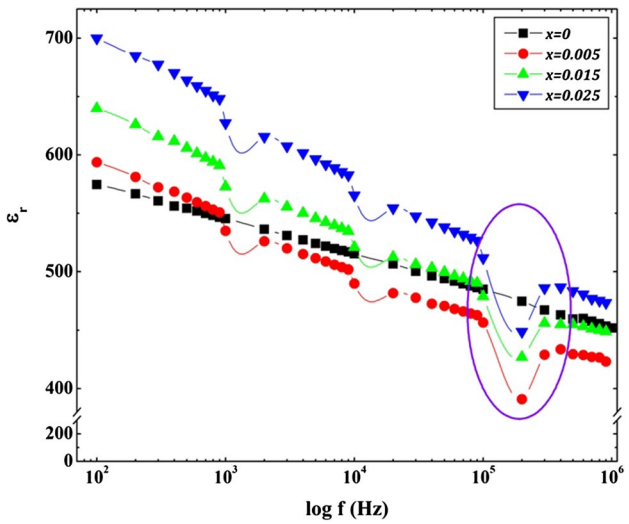

Fig. 5 Frequency dependent dielectric constant of $(1-x-y)$NBT–xBMT–yBMZ poled ceramics with various x

maximum tan δ value can be explained by Debye formula [32]. According to this formula tan δ is inversely proportional to frequency which explains the decrease in tan δ with the increase in frequencies beyond maximum [32, 33]. Room temperature dielectric constant decreases as the mole fraction of BMT substitution increases in NBT–BMZ solid solution. But a small increase in dielectric constant is seen for $x=0.025$ mole fraction of BMT. An increase in dielectric loss is seen up to $x=0.015$ mole fraction of BMT substitution, but a significant decrease in dielectric loss is noticed for $x=0.025$ mole fraction of BMT in NBT–BMZ system.

Figure 7 shows the temperature dependent dielectric constant and tangent loss of $(1-x-y)$ NBT–xBMT–yBMZ poled ceramics at 10 kHz. Two dielectric anomalies, in the region 150–220 °C and 310–380 °C are noticed due to ferroelectric to antiferroelectric transition and antiferroelectric to paraelectric phase transition with a Curie temperature respectively [34, 35] (Fig. 7a). Also a diffused phase transition is observed, which is a characteristic feature of perovskite based relaxor ferroelectrics due to the presence of different ionic radii and oxidation state cations namely Bi^{3+}, Na^{+} in the A-site and Mg^{2+}, Zr^{4+} and Ti^{4+} ions in the B-site of NBT [36–38]. The Curie temperature is found to be elevated to higher temperature from 320 to 345 °C in BMT substituted NBT–BMZ ceramics. Dielectric constant maximum at Curie temperature is highly enhanced for $x=0.025$ mole fraction of BMT substitution. Dielectric loss as a function of temperature indicates that

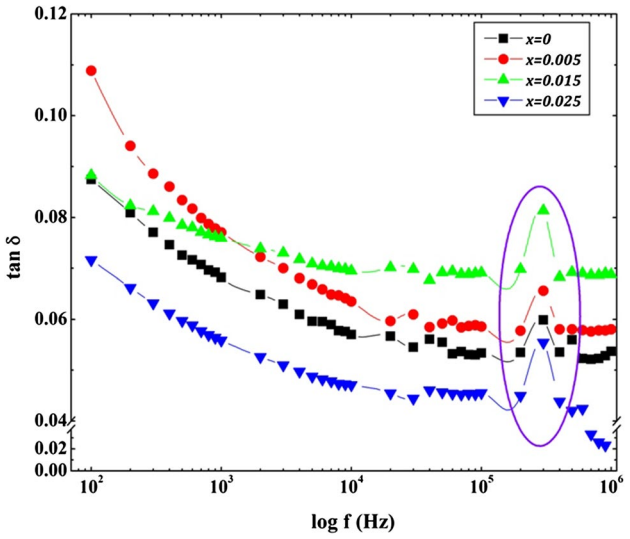

Fig. 6 Frequency dependent tan δ of $(1-x-y)$NBT–xBMT–yBMZ poled ceramics with various x

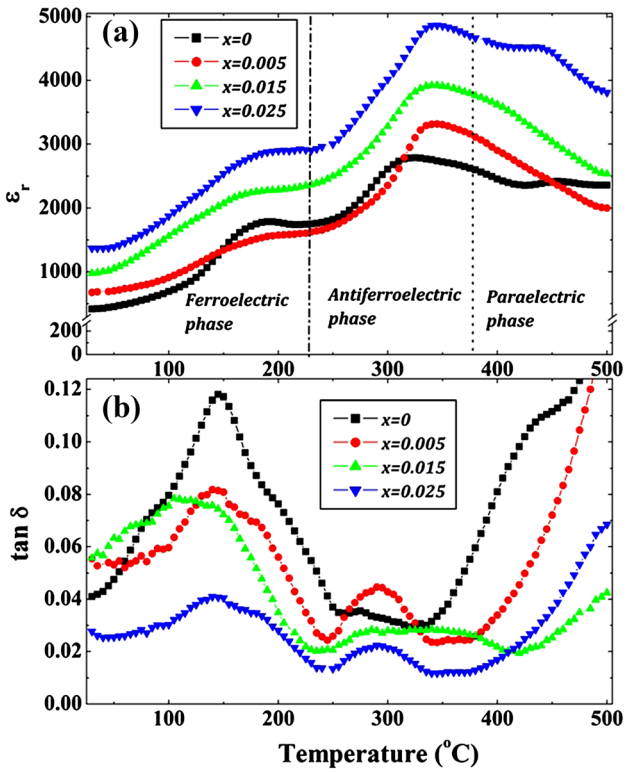

Fig. 7 Temperature dependent **a** dielectric constant, **b** tan δ of $(1-x-y)$NBT–xBMT–yBMZ poled ceramics with various x

substitution of BMT in NBT–BMZ ceramics drastically reduces the loss factor and at $x=0.025$ mole fraction of BMT substitution dielectric loss becomes minimum (as shown in Fig. 7b). Hence, from Fig. 7 it is found that dielectric constant is increased and tangent loss is greatly reduced for $x=0.025$ mole fraction of BMT substitution.

Room temperature (a) P–E hysteresis loop and (b) remnant polarization and coercive field of $(1-x-y)$ NBT–xBMT–yBMZ poled ceramics are shown in Fig. 8. Well saturated single loops are obtained for all mole fractions which indicate the ferroelectric nature of the samples (Fig. 8a). Both spontaneous polarization (P_s) and remnant polarization (P_r) increases on BMT substitution. On the other hand, the coercive field gradually decreases on BMT substitution (Fig. 8b) in NBT–BMZ solid solution. Reduction of coercive field in BNT–BMZ–BMT is similar to substitution of BKT in BNT–BT solid solution as reported earlier [16, 17].

Figure 9 shows the piezoelectric coefficient of $(1-x-y)$ NBT–xBMT–yBMZ poled ceramics as a function of mole fraction at room temperature. Piezoelectric coefficient (d_{33}) increases on BMT substitution in NBT–BMZ ceramics. Highest piezoelectric coefficient is obtained for $x=0.025$ mole fraction of BMT substitution in NBT–BMZ solid solution.

The major result drawn from the present work is that coercive field decreases in NBT–BMZ–BMT ternary system without reduction in remnant polarization (P_r) and piezoelectric coefficient (d_{33}). Homogeneous strain (δ) is the key intrinsic parameter which play a major role in the reduction of coercive field (E_c) in NBT–BMZ–BMT ternary system which maintains the rhombohedral structure symmetry. High dielectric constant and low dielectric loss is the principal requirement for energy storage devices such as capacitors to enhance the capacitance, increase the charge-storage efficiency and to minimize dissipation of stored energy into heat and further to reduce the draining of the stored charge [39]. Also, large remnant polarization and reduced coercive field is the principal requirement for ferroelectric memory devices [40]. Substitution of BMT ($x=0.025$ mole fraction) in NBT–BMZ system decreases the coercive field and dielectric loss than all other compositions. Moreover, the dielectric constant and remnant polarization are enhanced. A comparative bar diagram representing the electrical properties of NBT-based system shows enhancement in properties than binary systems.

Figure 10 shows the electrical properties of NBT–BMT, NBT–BMZ and NBT–BMT–BMZ poled ceramics. Table 1 gives the dielectric constant (ε_r), remnant polarization (P_r), piezoelectric coefficient (d_{33}), coercive field (E_c) and homogeneous strain (δ) of $(1-x)$NBT–xBMT, $(1-x)$ NBT–xBMZ and $(1-x-y)$NBT–xBMT–yBMZ lead-free piezoelectric solid solutions for the mole fraction which possess the better properties. From Fig. 10, it is found that in ternary system the coercive field is reduced than all the binary substitutions. It is evident that NBT–BMZ–BMT ternary system shows enhanced dielectric constant than

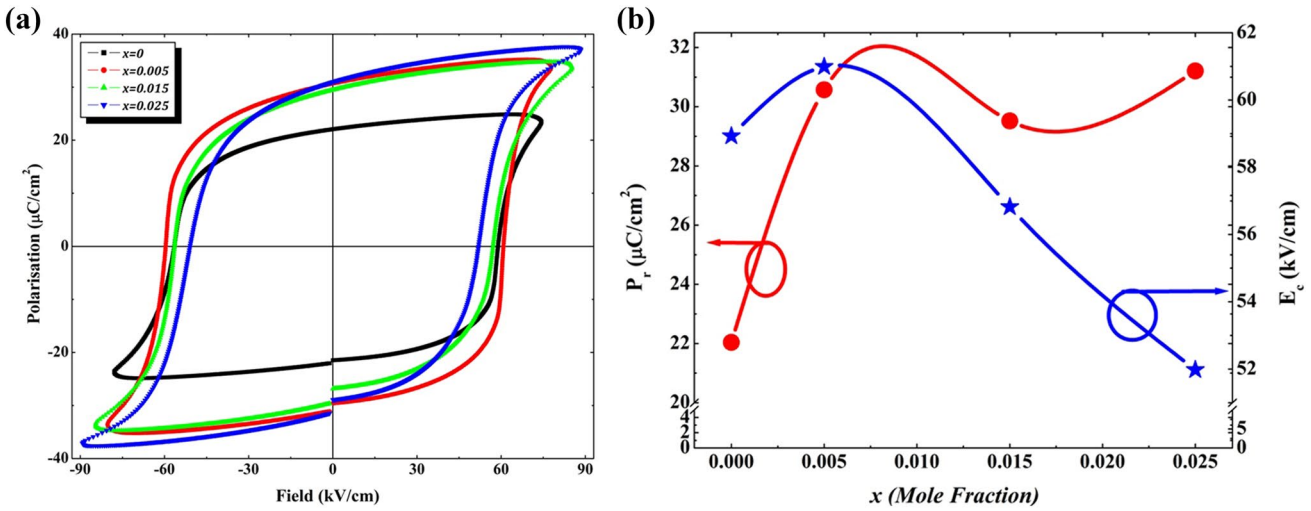

Fig. 8 **a** P–E hysteresis loop of $(1-x-y)$NBT–xBMT–yBMZ poled ceramics with various x. **b** Remnant polarisation (P_r) and coercive field (E_c) of $(1-x-y)$NBT–xBMT–yBMZ poled ceramics with various x

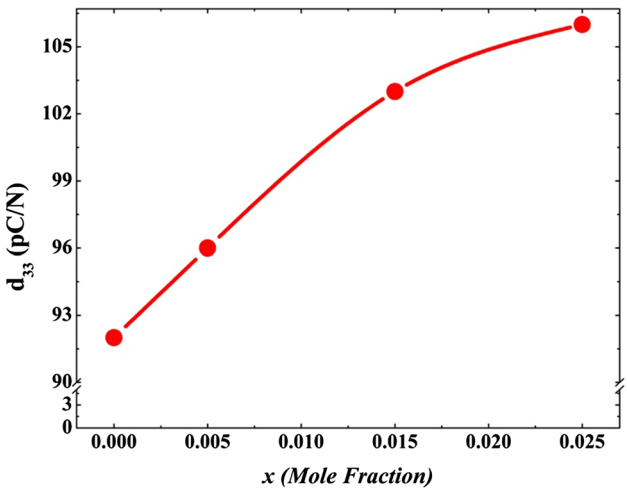

Fig. 9 Piezoelectric constant (d_{33}) of $(1-x-y)$NBT–xBMT–yBMZ poled ceramics with various x

other systems. At $x=0.025$ mole fraction of BMT substitution the dielectric constant is enhanced and dielectric loss is drastically reduced (Figs. 5, 6, 7). For the same composition the remnant polarization is increased and the coercive field is lowered. Decreased coercive field leads to low hysteresis loss. Therefore the hysteresis loss is decreased at $x=0.025$ mole fraction of BMT substitution than all other compositions. In ferroelectric ceramics low hysteresis loss, dielectric loss and enhanced dielectric constant are the prerequisite for storage devices [39, 40]. Hence these ceramics can be used for energy storage devices such as capacitors.

Piezoelectric researchers disclosed homogeneous strain as a decisive parameter for understanding the properties of piezoelectric ceramics in a complex manner [26]. From Table 1, it is noticed that comparably the homogeneous strain is decreased for NBT–BMZ–BMT ternary ceramics than the other two systems. Therefore, it is perceived that minimal homogeneous strain is the key for softening the coercive field in piezoelectric ceramics.

Lattice distortion and homogeneous strain plays a dominant role in enhancing the electrical properties of piezoelectric ceramics. But homogeneous strain is the basic intrinsic parameter which softens the coercive field and increases the dielectric constant in piezoelectric ceramics. Decrease in strain enhances the mobility of domains which in turn leads to decrease in coercive field. Hence substitution of BMT in NBT–BMZ ceramics softens the coercive field and enhances the dielectric constant.

This work provides a scope to soften the coercive field and enhanced dielectric constant with low loss in non-MPB based systems without deteriorating other electrical properties which is an essential requirement for application in functional devices.

4 Conclusion

NBT–BMZ–BMT ternary ceramics are synthesized by solid state reaction. Synthesized samples are phase pure and exhibits rhombohedral R3c symmetry. In NBT–BMZ–BMT ternary ceramics, the dielectric, ferroelectric and piezoelectric properties are enhanced. Interestingly, in NBT–BMZ–BMT ternary ceramics coercive field is reduced by increased mobility and improved domain switching without considerable decrease in remnant polarization and piezoelectric coefficient. Enhanced properties are achieved in NBT–BMZ–BMT due to small

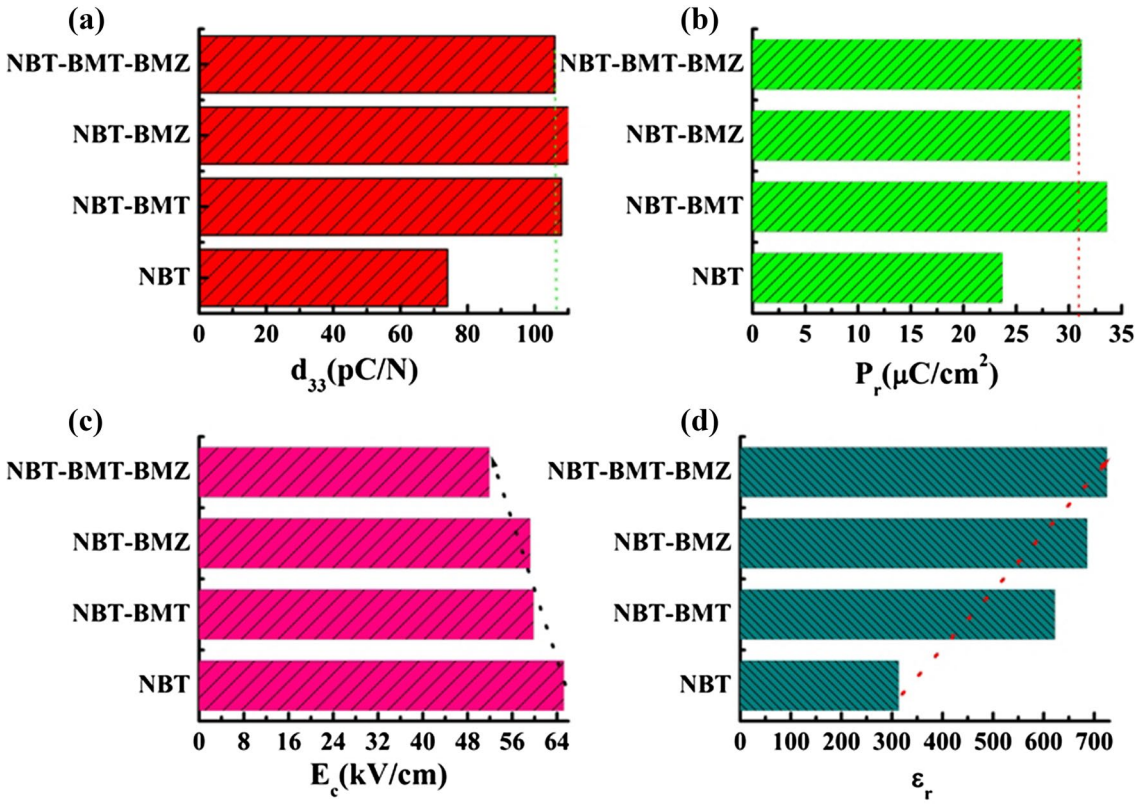

Fig. 10 Electrical parameters **a** piezoelectric coefficient, **b** remnant polarization, **c** coercive field, and **d** dielectric constant of NBT–BMT, NBT–BMZ and NBT–BMT–BMZ poled ceramics

Table 1 Electrical properties and homogeneous strain of NBT–BMT, NBT–BMZ and NBT–BMT–BMZ systems

NBT-based systems	Mole fraction, x	ε_r	P_r μC/cm^2	E_c kV/cm	d_{33} pC/N	90-α	Ref.
NBT	0	313.2	23.7	65.2	74	0.3465	[41]
NBT–BMT	0.04	687.3	33.6	58.3	108	0.2970	[14]
NBT–BMZ	0.01	686.2	30.5	59.2	112	0.2822	[15]
NBT–BMT–BMZ	0.025	725.3	31.2	51.5	105	0.2710	Present work

homogeneous strain. Therefore low homogeneous strain is the fundamental intrinsic parameter for softening of E_c in lead-free NBT-based systems.

Acknowledgements We thank the Council of Scientific and Industrial Research (CSIR), New Delhi, India, funding agency for the financial support under the Grant No. 03/(1238)/12/EMR-II.

References

1. Y. Saito, H. Takao, T. Tani, T. Nonoyama, K. Takatori, T. Homma, T. Nagaya, M. Nakamura, Nature **432**, 84–87 (2004)
2. J. Rodel, W. Jo, K.T.P. Seifert, E. Anon, T. Granzow, J. Am. Ceram. Soc. **92**(6), 1153–1177 (2009)
3. G.H. Haertling, J. Am. Ceram. Soc. **82**, 797–818 (1999)
4. P.K. Panda, J. Mater. Sci. **44**, 5049–5062 (2009)
5. M. Demartin Maeder, D. Damjanovic, N. Setter, J. Electroceram. **13**, 385–392 (2004)
6. S.O. Leontsev, R.E. Eitel, Sci. Technol. Adv. Mater. **11**, 044302 (2010)
7. E. Aksel, J.L. Jones, Sensors **10**, 1935–1954 (2010)
8. T.R. Shrout, S.J. Zhang, J. Electroceram. **17**, 111–124 (2007)
9. C.A. Randall, R. Eitel, B. Jones, T.R. Shrout, D.I. Woodward, I.M. Reaney, J. Appl. Phys. **95**, 3633 (2004)
10. G. Shabbir, A.H. Qureshi, S. Kojima, D.A. Hall, Ferroelectrics **346**, 72–76 (2007)
11. M.R. Suchomel, K.P. Davies, J. Appl. Phys. **96**, 4405 (2004)
12. Q. Wang, J. Chen, L. Fan, L. Liu, L. Fang, X. Xing, J. Am. Ceram. Soc. **96**, 1171 (2013)
13. A. Ullah, M. Ishfaq, C.W. Ahn, A. Ullah, S.E. Awan, W. Kim, Ceram. Int. **41**, 10557 (2015)
14. D.E. Jain Ruth, M. Muneeswaran, N.V. Giridharan, B. Sundarakannan, J. Mater. Sci. **27**, 7018–7023 (2016)

15. D.E. Jain Ruth, S.M. Abdul Kader, M. Muneeswaran, N.V. Giridharan, D. Pathinettam Padiyan, B. Sundarakannan, Ceram. Int. **42**, 3330–3337 (2016)
16. X.X. Wang, X.G. Tang, H.L.W. Chan, Appl. Phys. Lett. **85**(1), 91 (2004)
17. W. Chen, Y. Li, Q. Xu, J. Zhou, J. Electroceram. **15**, 229–235 (2005)
18. S.-T. Zhang, A.B. Kounga, E. Aulbach, T. Granzow, W. Jo, H.-J. Kleebe, J. Rödel, J. Appl. Phys. **103**, 034107 (2008)
19. E.-M. Anton, L.A. Schmitt, M. Hinterstein, J. Trodahl, B. Kowalski, W. Jo, H.-J. Kleebe, J. Rödel, J.L. Jones, J. Mater. Res. **27**(19), 2466 (2012)
20. Y.-M. Li, W. Chen, Q. Xu, J. Zhou, H.-J. Sun, M.-S. Liao, J. Electroceram. **14**, 53–58 (2005)
21. Y. Wu, H. Zhang, Y. Zhang, J. Ma, D. Xie, J. Mater. Sci. **38**, 987–994 (2003)
22. H. Yang, X. Shan, C. Zhou, Q. Zhou, W. Li, J. Cheng, Bull. Mater. Sci. **36**(2), 265–270 (2013)
23. B.N. Rao, R. Ranjan, Phys. Rev. **B86**, 134103 (2012)
24. E. Aksel, J.S. Forrester, J.L. Jones, P.A. Thomas, K. Page, M.R. Suchomel, Appl. Phys. Lett. **98**, 152901 (2011)
25. G.O. Jones, P.A. Thomas, Acta Cryst. **B58**, 168–178 (2002)
26. W. Heywang, K. Lubitz, W. Wersing, *Piezoelectricity Evolution and Future of a Technology, Springer Series in Materials Science* (Springer, New York, 2008)
27. J. Petzelt, S. Kamba, J. Fabry, D. Noujni, V. Porokhonskyy, A. Pashkin, I. Franke, K. Roleder, J. Suchanicz, R. Klein, G.E. Kugel, J. Phys. **16**, 2719 (2004)
28. J. Kreisel, P. Bouvier, J. Raman Spectrosc. **34**, 524 (2003)
29. J. Suchanicz, I. Jankowska-Sumara, T.V. Kruzina, J. Electroceram. **27**, 45 (2011)
30. M.K. Niranjan, T. Karthik, S. Asthana, J. Pan, U.V. Waghmare, J. Appl. Phys. **113**, 194106 (2013)
31. D.J. Griffiths, *Introduction to Electrodynamics*, 3rd edn. (Prentice Hall, Englewood, 1998
32. A.K. Singh, T.C. Goel, R.G. Mendiratta, O.P. Thakur, C. Prakash, J. Appl. Phys. **91**, 6626 (2002)
33. S. Chopra, S. Sharma, T.C. Goel, R.G. Mendiratta, Appl. Surf. Sci. **230**, 207 (2004)
34. W. Jo, J.E. Daniels, J.L. Jones, X. Tan, P.A. Thomas, D. Damjanovic, J. Rödel, J. Appl. Phys. **109**, 014110 (2011)
35. R. Ranjan, A. Dviwedi, Solid State Commun. **135**, 394–399 (2005)
36. G. Fan, W. Lu, X. Wang, F. Liang, J. Phys. D **41**, 035403 (2008)
37. S. Zhao, L. Zhang, G. Li, B. Li, A. Ding, Integr. Ferroelectr. **78**, 119–126 (2006)
38. J. Suchanicz, M.G. Gavshin, A.Y. Kudzin, C.Z. Kus, J. Mater. Sci. **36**, 1981–1985 (2001)
39. S. Krohns, P. Lunkenheimer, S. Meissner, A. Reller, B. Gleich, A. Rathgeber, T. Gaugler, H.U. Buhl, D.C. Sinclair, A. Loidl, Nat. Mater. **10**, 899–901 (2011)
40. L.E. Cross, *Ferroelectric Ceramics, Monte Verita* (Birkhiiuser Verlag, Basel, 1993), pp. 1–84
41. D.E. Jain Ruth, M. Veera Gajendra Babu, S.M. Abdul Kader, B. Bagyalakshmi, D. Pathinettam Padiyan, B. Sundarakannan, J. Mater. Sci. **26**, 6757–6761 (2015)